THE JOURNAL OF PHYSICAL CHEMISTRY C

Article

Cite This: J. Phys. Chem. C 2018, 122, 6463−6474

pubs.acs.org/JPCC

Inhomogeneous Photoluminescence Characteristic in Carbon Nanodots and Electrophotoluminescence Measurements

Morihiko Hamada,[†] Kenji Okoshi,[‡] Shailesh Rana,[†] Kamlesh Awasthi,[†] Toshifumi Iimori,[§] Eric Wei-Guang Diau,[†] and Nobuhiro Ohta*[,†]

[†]Department of Applied Chemistry and Institute of Molecular Science, National Chiao Tung University, 1001, Ta-Hsueh Road, Hsinchu 30010, Taiwan

[‡]Graduate School of Environmental Science, Hokkaido University, Sapporo 060-0810, Japan

[§]Department of Applied Chemistry, Muroran Institute of Technology, Muroran 050-8585, Japan

Supporting Information

ABSTRACT: Photoluminescence (PL) spectra, time-resolved PL spectra, and PL decay profiles have been observed for carbon nanodots (CDs) with different excitation wavelengths in an embedded solid film and in solution. PL excitation spectra have been also observed with different monitoring wavelengths. Then, it is found in both solid film and solution that not only the location of the PL spectra but also the peak of the excitation spectra show a significant red shift, as the excitation and monitoring wavelengths become longer, respectively, indicating that the emitting states of the excitation-dependent PL are the real state to which direct absorption occurs from the ground state, not the transient trapped states produced by photoexcitation. It is shown that not only the excitation-dependent PL but also the excitation-independent PL with a peak at ∼375 nm exist. The lifetimes of both PL emissions are very sensitive to the surroundings. Multiple emitting states that give excitation-dependent PL are ascribed to the inhomogeneous properties in prepared carbon nanodots, which is supported by the fluorescence lifetime image measurements. Electrophotoluminescence spectrum, that is, the electric-field-induced change in PL spectrum, has also been observed for the excitation-independent PL of CDs embedded in a poly(methyl methacrylate) film, and the magnitude of the change in electric dipole moment and molecular polarizability following emission has been determined.

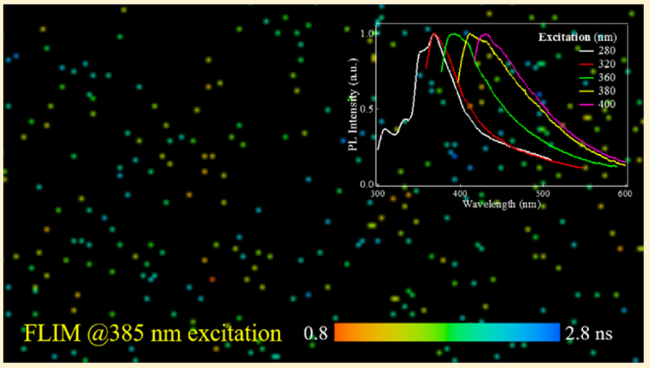

1. INTRODUCTION

As a new class of carbon nanomaterials, carbon nanodots (CDs), which have excellent properties associated with quantum confinement and edge effect, are emerging as promising optical materials for biological and optoelectronic applications due to their superiority during large optical absorptivity, chemical stability without photobleaching, biocompatibility, and low toxicity, as introduced in some review articles.[1−3] In particular, fluorescent CDs have been actively synthesized and applied in bioimaging and biosensing because of the lack of the above-mentioned problems, which are subject to restriction for biological application.[4−10] To date, many studies have focused on the synthesis methods of fluorescent CDs, and hydrothermal, solvothermal, and microwave synthesis methods are now currently common, and fluorescence properties of CDs with a narrow size distribution of 2−5 nm have been reported.[11−27]

Fluorescence spectra, lifetime, and quantum yield of CDs prepared by different methods have been reported; for example, fluorescence spectra of CDs prepared from poloxamar by a simple microwave-assisted process show a fluorescence peak at ∼442 nm with excitation at 380 nm with the average lifetime of 2.13 ns and the quantum yield of 7%.[11] As the excitation wavelength increases, the emission peak was shown to shift toward longer wavelengths. It has also been reported that CDs have a remarkably high photostability when CDs are used as a cell-imaging probe, suggesting that CDs can be used as efficient fluorescence probe in biological systems. Thus, the emission phenomena of CDs have been extensively examined with expectation as a nanoprobe, but the electronic structure of CD is still not clear and the mechanism of excitation-dependent emission is also the topic under debate.[28−30] In the present study, measurements of photoluminescence (PL) spectra, PL excitation (PL-EX) spectra, and PL decays of hydrophobic CDs embedded in a polymer film as well as in solution of chloroform and toluene have been carried out with excitation in a wide range of wavelength from 280 to 420 nm. Then, the presence of not only the excitation-wavelength-dependent emission but also

Received: January 24, 2018
Revised: February 23, 2018
Published: March 14, 2018

DOI: 10.1021/acs.jpcc.8b00841
J. Phys. Chem. C 2018, 122, 6463−6474

the excitation-wavelength-independent emission has been reported and the origin of multiple emitting states has been discussed.

Electric dipole moment and molecular polarizability are typical physical parameters that characterize the electronic structure of molecules and materials. These parameters are strongly related to the molecular structure and molecular dynamics, including the emission process in each state. These physical parameters also play an important role in optoelectronic function, such as nonlinear optical property or electron injection/accepting properties. These physical properties can be estimated from the analysis of the Stark shift of the optical spectra. When CDs are used as a fluorescent probe in biological system, further, it may be important to know how the emission property is affected by electric field because a strong local field may exist in the biological system where CDs are located.[31−33] In the present study, we have examined the effect of electric field on the absorption and PL spectra of hydrophobic CDs fabricated from a poloxamer. In the results, the magnitude of change in the electric dipole moment and molecular polarizability following emission has been estimated for the excitation-independent PL on the basis of the electric field effect on the PL spectra.

2. EXPERIMENTAL SECTION

CDs were synthesized by following the previously reported method with a slight modification.[11] Poly(oxyethylene)−poly(oxypropylene)−poly(oxyethylene) block co-polymer Kolliphor P188 (Aldrich, 60 mg) was added to distilled water (5 mL) and stirred for 15 min. Phosphoric acid (10 mL) was added to the aqueous solution and stirred for 10 min. The mixture was heated for 4 min using a domestic microwave oven at 400 W and cooled to room temperature. Then, distilled water (25 mL) was added and the solution was stirred for 10 min. CDs were extracted by using chloroform or toluene (20 mL). The solution was evaporated to dryness and then chloroform or toluene (2.5 mL) was added to obtain CD solution. For characterization, transmission electron microscopy (TEM) images of the CDs were collected on a JEOL JEM-2100XS transmission electron microscope using 200 kV acceleration voltage. Specimens were prepared by slowly vaporizing a drop of the CDs dispersion in chloroform solution on a carbon-coated grid. X-ray diffraction (XRD) (Rigaku Corporation, MultiFlex-120NP) analyses were carried out with the film of CDs prepared by dropping the CDs solution in toluene on the substrate.

A certain amount of toluene solution or chloroform solution of CD and poly(methyl methacrylate) (PMMA, Aldrich; average molecular weight, 120 000) purified by precipitation with toluene and methanol was cast on an indium tin oxide (ITO)-coated quartz substrate by a spin-coating method. Then, a semitransparent aluminum (Al) film or silver (Ag) film was deposited on the polymer film by a vacuum vapor deposition technique. The ITO and Al or Ag films were used as electrodes.

The steady-state absorption and PL spectra were recorded by an absorption spectrometer (Hitachi, U-3500 or JASCO, V670) and a fluorescence spectrometer (JASCO, FP-777), respectively. Continuous irradiation was carried out with a 150 W Xe lamp in combination with a monochromator and neutral density filters.

All of the optical measurements were performed at room temperature. Electroabsorption (E-A) and electrophotoluminescence (E-PL) spectra were measured by electric field modulation spectroscopy with the same apparatus as described elsewhere.[34,35] A modulation in absorption intensity or PL intensity was induced by a sinusoidal alternating-current voltage with a modulation frequency of 40 Hz. Field-induced change in absorption intensity or PL intensity was detected with a lock-in amplifier at the second harmonic of the modulation frequency (40 Hz). A direct-current component of the transmitted light intensity or the PL intensity was simultaneously observed. E-A and E-PL spectra were obtained by plotting the change in absorption intensity and PL intensity as a function of wavenumber, respectively. The angle between the direction of the applied electric field and the electric vector of the excitation light was set to the magic angle (54.7°) in the E-A measurements, and depolarized emission was detected in the E-PL measurements. Applied field strength was evaluated from the applied voltage divided by the thickness of the sample, i.e., the distance between two electrodes. Hereafter, applied electric field is denoted by F.

PL decay profiles of CDs in both a PMMA solid film and solution were measured with a single-photon counting method.[36] The second harmonic (380 and 400 nm) or the third harmonic (280 nm) of the output from a mode-locked Ti:sapphire laser (Spectra Physics, Tsunami) was used for excitation. The pulse width of the excitation light was about 100 fs. The repetition rate was reduced to be ∼6 MHz with a pulse picker (Conoptics, model 350-160) from the original 81 MHz. In the decay measurements, PL dispersed with a monochromator (Nikon, G-250) was detected with a microchannel-plate photomultiplier (Hamamatsu, R3809U-52). The PL signal was discriminated from thermal noises and then led to a time-to-amplitude converter system. PL decays were obtained with a multichannel pulse height analyzer (SEIKO EG&G, model 7700). The instrumental response function had a pulse width of ∼60 ps (full width at half-maximum). By combining the decays at different monitoring wavelengths observed with the same accumulation time, time-resolved PL spectra could be obtained. Before the measurements of time-resolved PL spectra, the PL spectrum was obtained in a short time by counting the total emission intensity at each monitoring wavelength under the same experimental condition. The resulting spectrum, which is called hereafter as the total PL spectrum, was shown in the computer display. After the decay measurement at each monitoring wavelength, the integrated intensity of the decay was shown in the display, together with the total PL spectrum. By comparing the total PL spectrum with the PL spectrum obtained from the integrated intensity of the decay as a function of monitoring wavelength, it was confirmed that photobleaching was negligible in solution. In the measurements of the time-resolved PL spectra in a PMMA film, the sample plate was slightly moved at each monitoring wavelength, that is, the irradiation position was slightly changed at each monitoring wavelength to protect photobleaching.

Fluorescence lifetime microscopy (FLIM) images of CDs embedded in a PMMA solid film were obtained using an inverted microscope (Nikon, TE2000E) through an objective lens (40×) with a time-correlated single-photon counting system (Becker & Hickl GmbH, SPC-830).[37,38] The second harmonic output from a mode-locked Ti:sapphire laser (385 nm) was used as excitation light. PL of CDs was detected by a microchannel-plate photomultiplier tube (Hamamatsu, R3809U) in the region of 417−477 nm. Analysis of the FLIM data was performed with SPC image software (Becker & Hickl GmbH).

DOI: 10.1021/acs.jpcc.8b00841
J. Phys. Chem. C 2018, 122, 6463−6474

3. RESULTS AND DISCUSSION

3.1. Photoluminescene (PL) Properties of CDs in a PMMA Solid Film and in Solution. As shown in the TEM image of the synthesized CDs shown in Figure 1, CDs are not

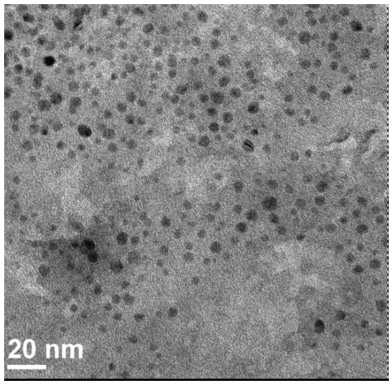

Figure 1. TEM image of carbon nanodots.

uniform, but their diameter is roughly 5 nm. The contrast of the TEM image may show a nonuniform distribution of the dispersed CDs when chloroform solution of CDs was just dropped on carbon-coated TEM grid and dried as the sample preparation for the TEM image measurements. The presence of dark particles may be due to the accidental overlap of CDs, which induces the different heights of CDs from the surface. As shown in Supporting Information (Figure S1), the X-ray diffraction pattern of CDs shows a broad band centered at 2θ = ~23°, indicating the (002) plane of carbon with poor crystallinity or nearly amorphous nature.[11]

PL spectra of CDs embedded in a PMMA solid film were observed with excitation wavelength (λ_{ex}) in the range of 280–420 nm, and the results are shown in Figure 2. PL spectra of CDs have also been measured in chloroform solution and toluene solution to compare the PL spectra of CDs embedded in a PMMA film with the ones in solution (see Figure 2). Mitra et al. already reported the PL spectra of CDs in chloroform and in solution,[11] but λ_{ex} in their experiments was limited to the ones longer than 330 nm. As mentioned later, excitation at wavelengths shorter than 330 nm has important implication in the sense that PL observed with λ_{ex} shorter than 320 nm shows different property from the one with λ_{ex} longer than 320 nm, regarding the excitation wavelength dependence of the PL spectra. In agreement with the results reported so far, the PL spectra depend on λ_{ex}, and the peak position of the PL spectra shifts to the red region, as λ_{ex} becomes longer in both a solid film and solution. It is noted that a cut filter was used to eliminate the scattered light during the measurements, which originates from reflection as well as Rayleigh scattering of the excitation light, and the spectra shown in Figure 2 have been corrected for the filter by using the transmittance spectra of the filter employed.

As shown in Figure 3, plots of the peak position of the PL spectrum as a function of λ_{ex} clearly show that PL peaks shift to the red region as λ_{ex} becomes longer. However, careful look of the plots in Figure 3 tells us that PL peak is roughly independent of λ_{ex} when λ_{ex} is shorter than 320 nm, whereas a monotonic increase of the red shift with increasing λ_{ex} is observed in the excitation wavelength region longer than 320 nm. These results indicate that different PL components exist in both solution and a solid film; one component that shows

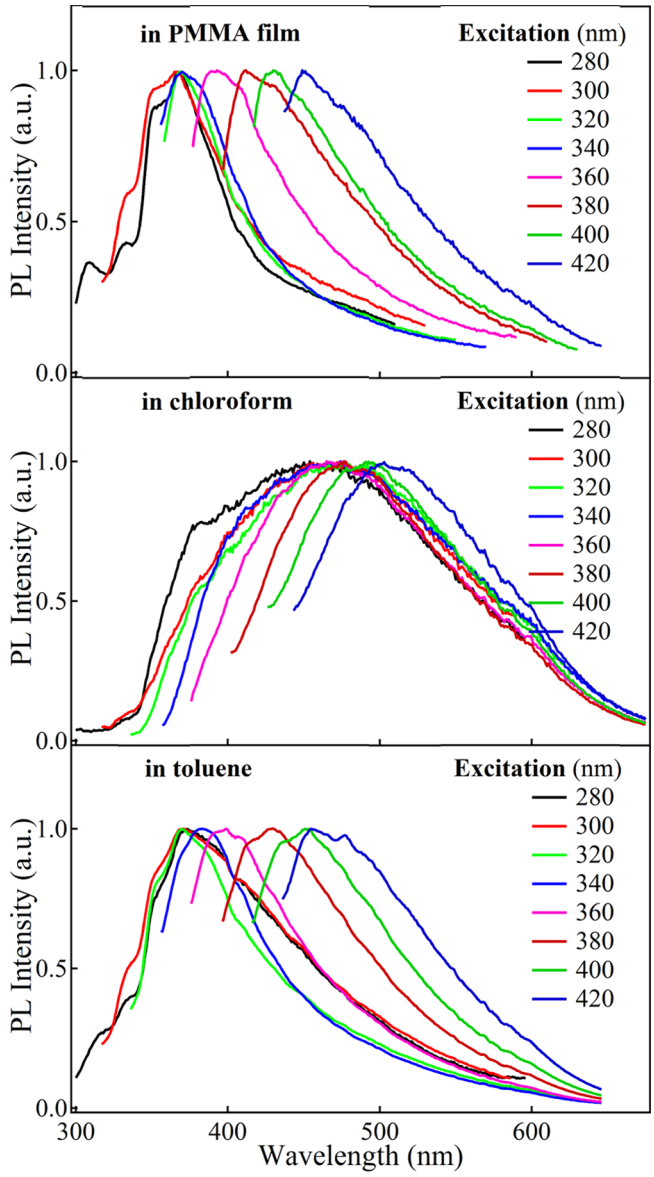

Figure 2. PL spectra of CDs in a PMMA solid film (top), in chloroform (middle), and in toluene (bottom) observed with different excitation wavelengths. The spectra are normalized at the maximum intensity.

the PL peak at around 375 nm is independent of λ_{ex}, whereas another component that is observed with λ_{ex} longer than 320 nm shows a red shift with increasing λ_{ex}. Hereafter, these λ_{ex}-independent and -dependent PL components are denoted as PL(I) and PL(II), respectively. The peak position of the PL spectra of CDs in chloroform is located in much longer-wavelength region than that in a PMMA film or in toluene. As shown in Figure 2, however, PL spectra of CDs in chloroform show a shoulder at around 375 nm with excitation at 280 or 300 nm, indicating that the PL component, which is similar to PL(I) observed in a PMMA film or in toluene, exists even in chloroform solution, and the peak position only of PL(II) is considered to show a significant solvent effect.

PL excitation spectra of CDs have also been observed in a PMMA solid film and in solution by monitoring the PL at different wavelengths. The results are shown in Figure 4. PL excitation spectra of CDs in the wavelength region shorter than

DOI: 10.1021/acs.jpcc.8b00841
J. Phys. Chem. C 2018, 122, 6463–6474

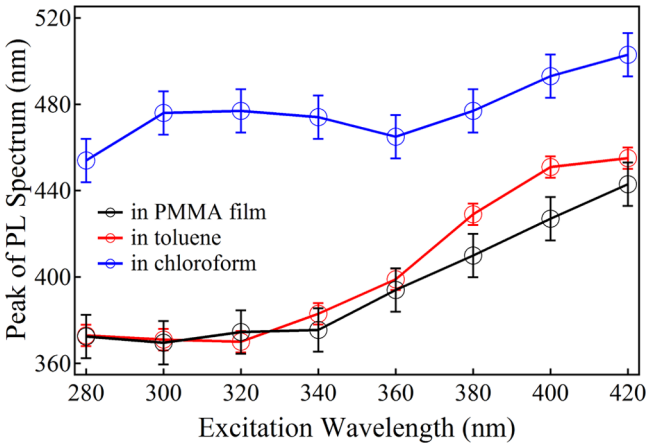

Figure 3. Plots of the wavelength at the peak of the PL spectra as a function of excitation wavelength in a PMMA solid film, in chloroform, and in toluene.

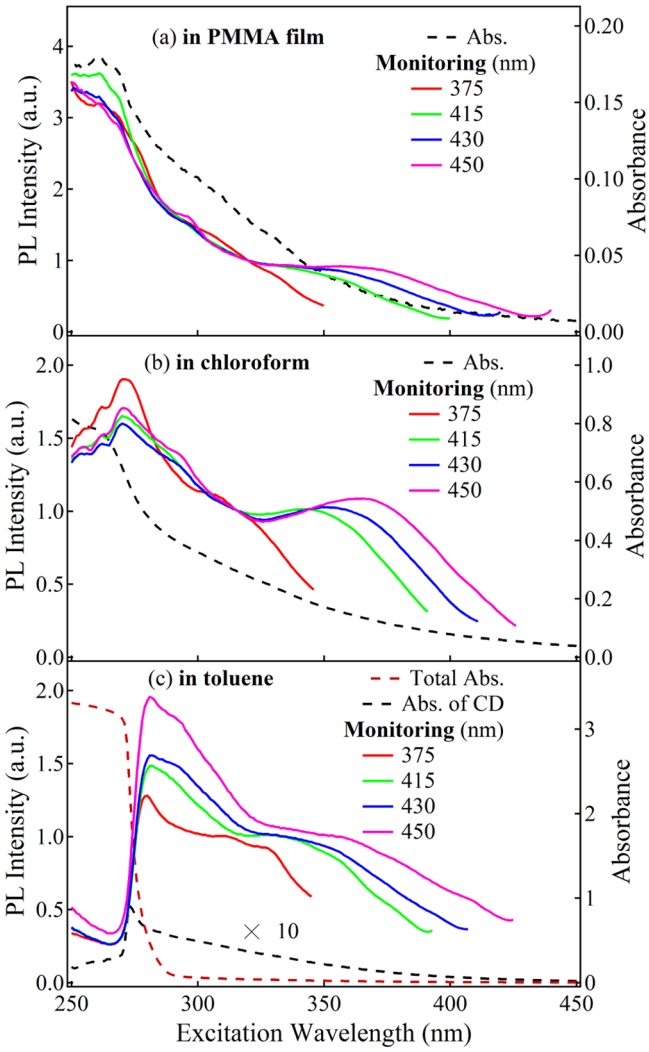

Figure 4. PL excitation spectra of CDs in a PMMA solid film (a), in chloroform (b), and in toluene (c) obtained by monitoring PL at different wavelengths. The spectra are normalized at the intensity at 320 nm in (a) and (b) and at the intensity of the broad band located in the longer-wavelength region in (c).

300 nm, where vibrational structure is observed, are roughly the same even with different monitoring wavelengths in both a solid film and chloroform, although this could not be confirmed in toluene because of the inner filter effect. Because toluene has a very strong absorption intensity in the short-wavelength region, the correction to the inner filter effect could not be done correctly, and so the reliable PL excitation spectrum could not be obtained in toluene solution in the shorter-wavelength region at around 280 nm. Thus, the sudden drop of the intensity of the PL excitation spectrum in toluene in the shorter-wavelength region in Figure 4 is due to the inner filter effect.

In the present results of the PL excitation spectra, it is stressed that the observed excitation spectra of CDs are very different from the ones reported so far, in the sense that the excitation spectra show a strong intensity even at wavelengths shorter than 300 nm even when the PL at wavelengths longer than 400 nm was monitored. In most of the spectra reported so far, excitation spectra show a mirror image of the PL spectrum, and the PL intensity is very weak with excitation at ~300 nm.[8,9,19−21,29,30,39−43] If so, the emission quantum yield of CDs remarkably depends on the excitation wavelength, indicating that the quantum yield is extremely low with excitation into higher electronic state of CDs. It is well known as Kasha's rule that energy transfer from higher electronic state to the lowest excited state (emitting state) is very fast, i.e., intramolecular internal conversion process is extremely fast. In the result, the emission quantum yield is usually independent of the excitation wavelength and the emission excitation spectrum is essentially the same in shape as the absorption spectrum. If the intensity of the emission excitation spectrum of CDs in the short-wavelength region is very low, as reported in many papers, then the emission property as well as relaxation process of CDs contradicts Kasha's rule, in contrast to usual polyatomic molecules. As far as the PL excitation spectra observed in the present study are concerned, however, the shape of the PL excitation spectra seems to follow the absorption spectra even in the short-wavelength region, although different species of CDs that give different absorption spectra exist in the present samples in both solution and polymer film, as described below. Even in CDs, therefore, Kasha's rule seems to hold as the fast relaxation dynamics from the photoexcited state to the emitting state.

On the basis of the time-resolved emission measurements in water and dimethylformamide, excitation-dependent emission was attributed to inhomogeneous broadening and spectral migration by the slow relaxation of the solvent molecules around CDs, not from a quantum confinement due to the mixture of particles or the presence of multichromophoric groups.[29] On the other hand, Sharma et al. reported the excitation-wavelength-dependent PL of CDs, and discrete multiple electronic states, which are assigned to the presence of different types of aggregates even at very dilute solution, were suggested to be involved in the excitation-dependent emission of carbon nanodots, based on the steady-state and time-resolved photoluminescence spectroscopy, including the anisotropy measurements in water and ethanol.[30] They measured PL spectra only with excitation at wavelengths longer than 350 nm, and so the excitation-wavelength-independent PL observed in the present experiments with excitation at wavelengths shorter than 320 nm was not referred.

In the PL excitation spectra shown in Figure 4, a distinct broad band, whose peak is located at wavelengths longer than

DOI: 10.1021/acs.jpcc.8b00841
J. Phys. Chem. C 2018, 122, 6463−6474

325 nm, is clearly observed, in addition to the strong bands located in the wavelength region shorter than 300 nm. This broad band shows clear monitoring wavelength dependence in any sample, that is, this peak shifts to the red as the monitoring wavelength becomes longer. Plots of the peak position of the PL excitation spectra in a PMMA film and in solution are shown in Figure 5 as a function of monitoring wavelength,

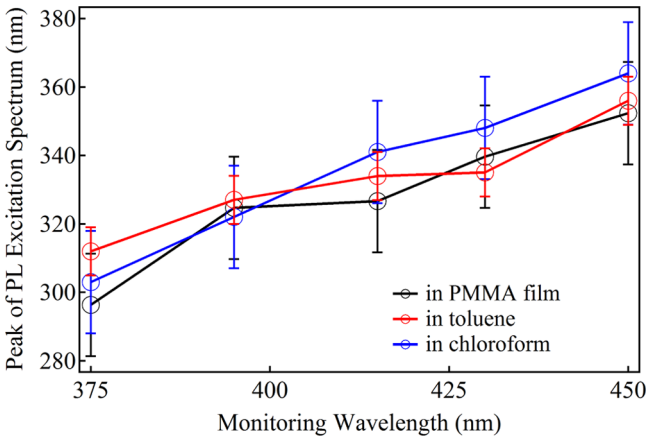

Figure 5. Plots of the wavelength at the peak of the PL excitation spectra located in the longer-wavelength region as a function of monitoring wavelength in a PMMA solid film, in toluene, and in chloroform.

which shows a monotonic red shift of the peak position with increasing monitoring wavelength. These results clearly show that the red shift of the PL spectra with increasing excitation wavelength results from the presence of multiple photoexcited states. These results are in agreement with those of Sharma et al.,[30] as far as PL(II), which is observed with excitation at wavelengths longer than 330 nm, is concerned. They suggested the presence of different types of aggregates even at very low dilute solutions[30] as the origin of the involvement of the multiple electronic states for the excitation-dependent emission in CDs. However, their speculation is doubtful because aggregates are not confirmed in the TEM image shown in Figure 1, and it is considered that CDs show different absorption and emission spectra from each other even without making aggregates. As shown in the emission excitation spectra given in Figure 4, the absorption spectra consist of the shorter-wavelength band with a peak at around 270 nm (band I) and the broad band located at wavelengths longer than 300 nm (band II). A comparison between absorption spectrum and PL excitation spectrum implies that the absorption intensity ratio between band I and band II depends on CD and that CDs with stronger absorption intensity for band II show higher PL quantum yield.

The spectra of the excitation-wavelength-dependent PL, i.e., PL(II) spectra, show a very different peak in chloroform from the one in a PMMA film or in toluene (see Figures 2 and 3), indicating that the location of the emitting state of PL(II) is very sensitive to the surroundings. Then, the PL(II) may remind the emission from the surface-trapped state.[44] However, it should be noted that the emitting state of PL(II) is the real state to which direct absorption occurs from the ground state, not the transient states produced by photoexcitation. The multiple emitting states that show different absorption bands

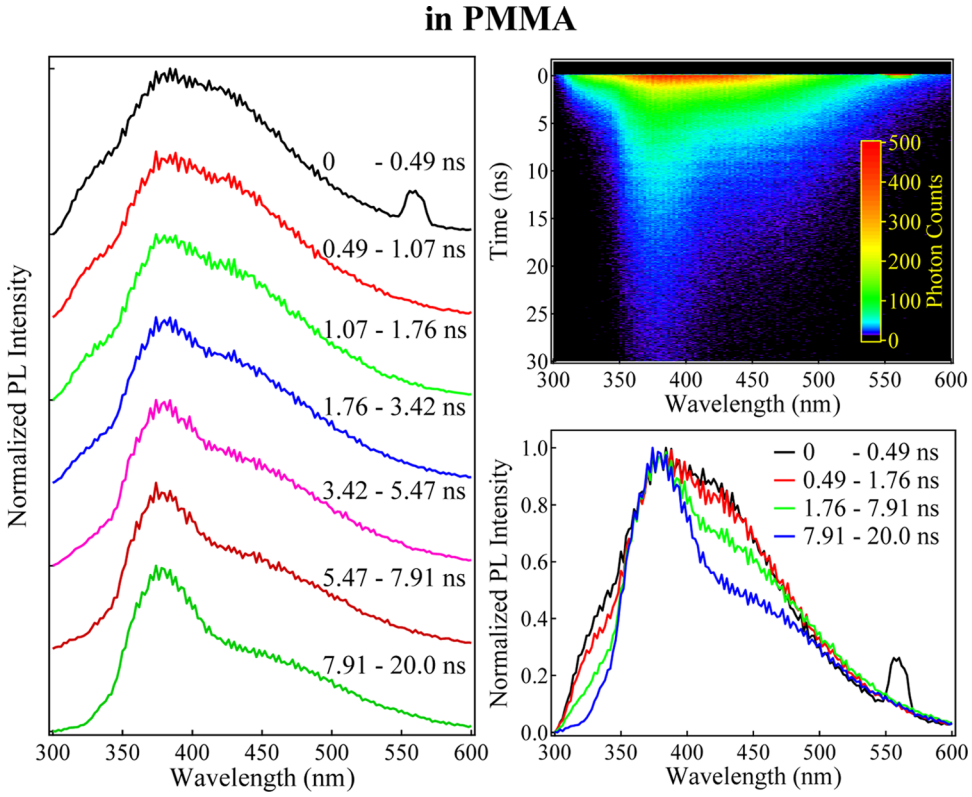

Figure 6. Time-resolved PL spectra (left) of CDs in a PMMA film, where the time range for each spectrum is shown in the figure; time-resolved intensity image (right, upper); and normalized time-resolved PL spectra (right, lower). The peak at ~560 nm observed with a time range of 0−0.49 ns results from the second harmonic of the scattering of excitation light.

DOI: 10.1021/acs.jpcc.8b00841
J. Phys. Chem. C 2018, 122, 6463−6474

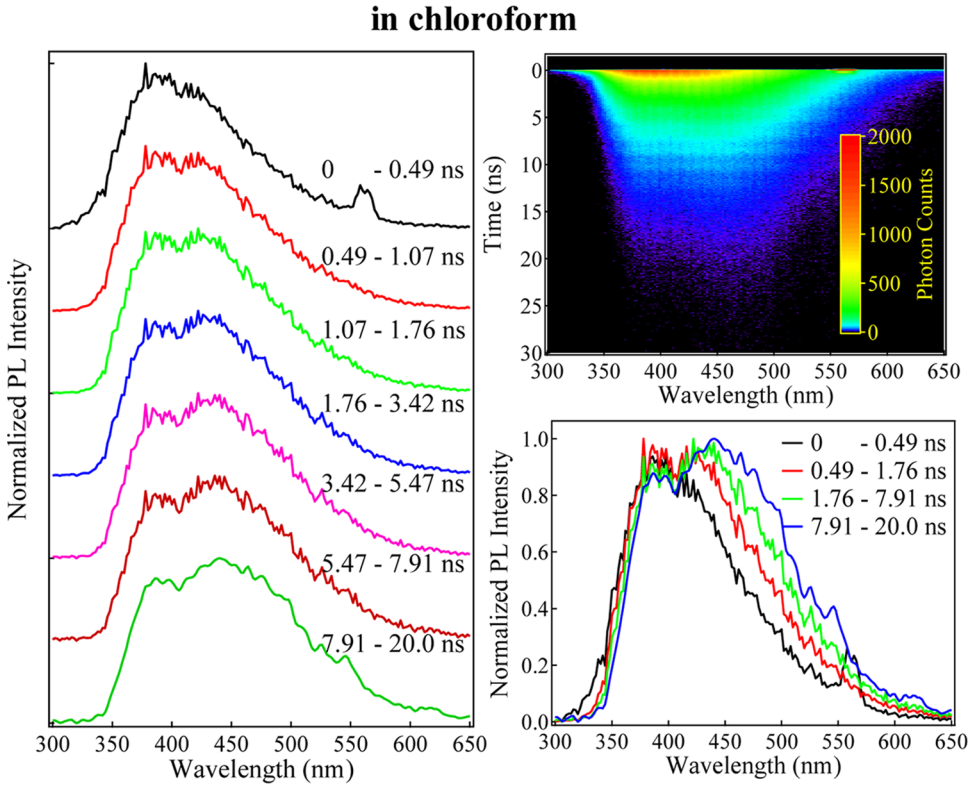

Figure 7. Time-resolved PL spectra (left) of CDs in chloroform, where the time range for each spectrum is shown in the figure; time-resolved intensity image (right, upper); and normalized time-resolved PL spectra (right, lower). The peak at ~560 nm observed with a time range of 0−0.49 ns results from the second harmonic of the scattering of excitation light.

from each other may originate from different modification of the surface states of CDs.[45] The fact that the absorption band II, which corresponds to the emitting state of PL(II), is very broad in structure and also very sensitive to the surrounding may imply that this absorption band has a kind of charge-transfer character from the core part of the carbon network to the surface state. In contrast to PL(II), PL(I), which is observed with excitation into higher excited state and nearly independent of the excitation wavelength, may originate from the state composed of the core part of the sp^2-carbon networks. Further, the emitting state of PL(I) may be related to the state where −COOH and/or −OH groups are ionized because the emission at ~375 nm was dominant at very low proton concentration, i.e., pH > 10.[29] In contrast to the location of the emitting state, the relaxation dynamics at the emitting state significantly depends on the surrounding in both PL(I) and PL(II), as the PL decays show.

Time-resolved PL spectra were obtained with excitation at 280 nm in solution and in a PMMA film. The results in a PMMA film and in chloroform are shown in Figures 6 and 7, respectively. We note that the time-resolved PL spectra obtained with excitation at 280 nm in toluene are quite similar to the ones in a PMMA film, as shown in Supporting Information (Figure S2). Besides the strong peak at ~375 nm, which can be assigned to PL(I), another band located at longer wavelengths is clearly seen in every sample, which is assigned to PL(II). PL(I) decays faster in chloroform than in a PMMA film or in toluene, whereas it decays slower in toluene or in a PMMA film than in chloroform. Khan et al. reported that PL spectra of CDs showed inhomogeneous broadening due to the slower relaxation of the solvent molecules.[29] As far as the present time-resolved PL spectra are concerned, spectral broadening with excitation at 280 nm results from the overlap of different bands, i.e., PL(I) and PL(II), and the spectral migration of both bands as a function of passage of time is not significant. It is also known that there is another component of PL at around 330 nm, which decays much faster than PL(I) and PL(II). In contrast to excitation at 280 nm, time-resolved PL spectra with excitation at longer wavelengths, i.e., 400 nm, show only one peak at around 465−485 nm (see time-resolved PL spectra in chloroform shown in Supporting Information (Figure S3)). Even with excitation at 400 nm, spectral migration as a function of passage of time is not significant, as in the case with excitation at 280 nm, although a slight Stokes shift is observed.

PL decays of CDs have been measured in both a PMMA film and solution with excitation at 280, 380, and 400 nm, and the results are shown in Figure 8. The decay measurements with excitation at 280 nm were performed at monitoring wavelengths of 330, 375, and 450 nm because time-resolved PL spectra clearly show that decay profiles at these monitoring wavelengths are different from each other (see Figures 6, 7, and S2). With excitation at 380 and 400 nm, decays were measured at only one monitoring wavelength because only one peak is confirmed in the PL spectra with these excitations. The observed decays were simulated by assuming a triexponential decay, i.e., $I(t) = \sum_i C_i \exp(-t/\tau_i)$, where i = 1, 2, and 3. The lifetime (τ_i) and pre-exponential factor (C_i) of each component of the simulated decays as well as the average lifetime ($\tau_{av} \equiv \sum_i C_i\tau_i/\sum_i C_i$) are shown in Table 1. As mentioned above, PL observed at 375 nm with excitation at 280 nm is denoted as PL(I), whereas PL observed at 430 or 450 nm is denoted as PL(II). In any sample, the PL decay profile depends on the excitation wavelength, indicating that different emitting states

DOI: 10.1021/acs.jpcc.8b00841
J. Phys. Chem. C 2018, 122, 6463−6474

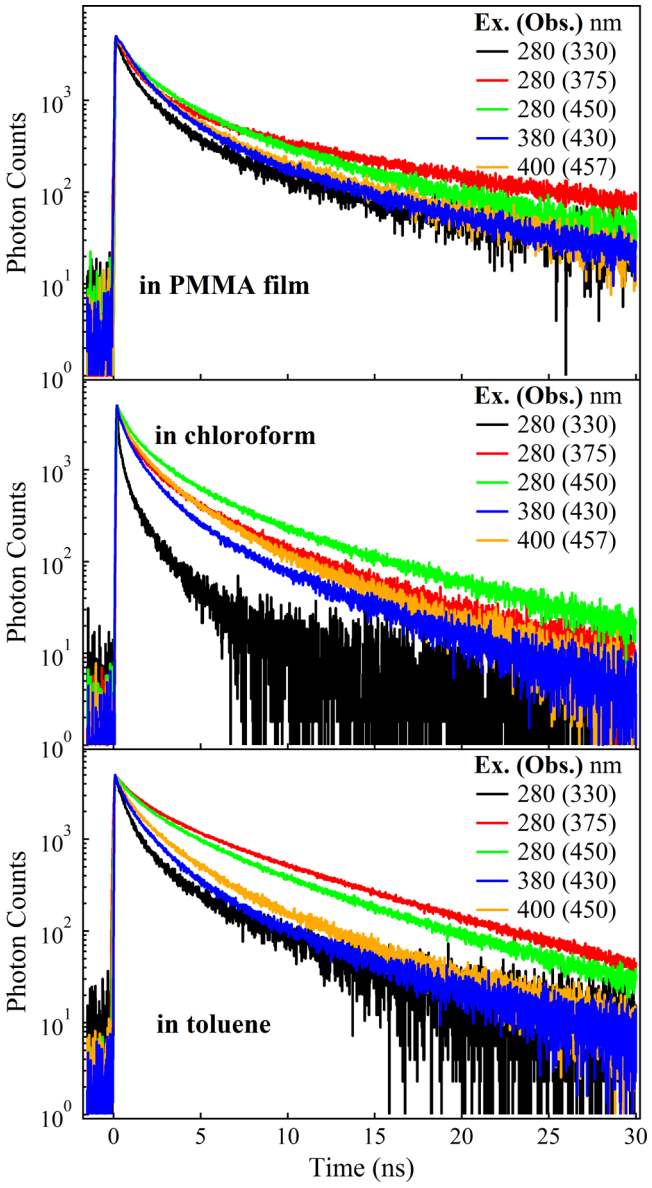

Figure 8. PL decay profiles of CDs in a PMMA solid film (top), in chloroform (middle), and in toluene (bottom) observed with excitation at different wavelengths. The PL intensity was monitored at 330, 375, 450, 430, and 457 (or 450) nm with excitation at 280, 280, 280, 380, and 400 nm, respectively.

are produced with different excitation wavelengths, in agreement with the PL excitation spectra, which depend on the monitoring wavelength.

The presence of different PL components, i.e., PL(I) and PL(II), with excitation at 280 nm is confirmed from the time-resolved PL spectra of CD in both solution and a PMMA film, as already mentioned. PL(I) at 375 nm with excitation at 280 nm shows a large value of τ_{av} in toluene (3.37 ns) and in a PMMA film (2.73 ns). In chloroform, τ_{av} (1.38 ns) and the lifetime of each component of PL(I) are much shorter than those in a PMMA film and in toluene. In the results, τ_{av} of PL(II) at ~450 nm with excitation at 280 nm is much longer than τ_{av} of PL(I) in chloroform, whereas τ_{av} of PL(II) is shorter than τ_{av} of PL(I) in toluene and in a PMMA film, as confirmed in Figures 6, 7, and S2. The results in toluene or in a PMMA film clearly show that the emitting states of PL(II) are not produced by the relaxation from the emitting state of PL(I). τ_{av} of PL(II) with excitation at 280 nm is shorter in chloroform than in toluene or PMMA film, indicating that the nonradiative decay at the emitting states of both PL(I) and of PL(II) with excitation at 280 nm is much faster in chloroform than in PMMA film or in toluene.

In agreement with the time-resolved PL spectra shown in Figures 6, 7, and S2, PL at 330 nm with excitation at 280 nm decays much faster than PL at any other monitoring wavelengths. Especially, the lifetime of PL at 330 nm in chloroform is much shorter than in toluene or in a PMMA film. This fast-decaying component may be attributed to hot luminescence emitted from higher vibrational levels produced by the relaxation from the photoexcited state. It is also known that the lifetime of PL with excitation at 380 or 400 nm is much shorter in chloroform than in others and that the lifetime of the corresponding PL in toluene is longer than in a PMMA film. These relations mainly result from the difference in lifetime of the fast-decaying component (see Table 1).

As the origin of multiplex emitting states, two possibilities may be considered: (1) the presence of different types of aggregates even in very low dilute solution or even in a diluted embedded film, as suggested by Sharma et al.[30] and (2) the presence of different subsets of CDs due to sample heterogeneity, as suggested by Ghosh et al.[28] In the present experiments, it could be confirmed that excitation dynamics of CDs is different from each other. Aggregates of CDs are not seen in the TEM image (see Figure 1). Then, it is unlikely that CDs make some aggregates even at low concentration in chloroform because the TEM image was taken for the CDs dispersed on the plate from chloroform solution. Therefore, it is strongly suggested that CDs show very different excitation dynamics from each other because of the heterogeneous property of the CDs even without formation of aggregates. FLIM measurements also support that CDs show different photoexcitation dynamics from each other. It is very likely that CDs give different energy levels as well as different absorption and PL spectra from each other. As shown in Figure 9, each spot seems to show a single exponential decay with different lifetimes, in agreement with Ghosh et al.[28] Actually speaking, it is not certain in the present results shown in Figure 9 whether emission at each spot shows a single exponential decay or not because of the low signal-to-noise ratio, which comes from low PL intensity. However, the present results clearly show that the lifetime is not the same in different QDs, indicating heterogeneous PL characteristics in the sense that each CD shows different photoexcitation dynamics from each other. This result indicates that the multiexponential decay of the bulk solution observed in Figure 8 comes from the ensemble averaging of inhomogeneous lifetimes shown by different CD particles.

It has been suggested that hydroxyl and carbonyl groups on the surface of the CDs resulted in the formation of defect sites[46] and emissive traps,[14] which contributed to its PL properties. Surface functionality of present CDs may be clarified from the FTIR spectra reported by Mitra et al.,[11] which suggested that the synthesized CDs comprised −OH groups, C−H groups (asymmetric and symmetric stretching), carbonyl, C−O, and C−O−C groups because the present samples of CDs were synthesized by a similar method. The surfaces composed of hydroxyl and carbonyl groups may induce the sample heterogeneity in the present CDs, resulting in the multiplex emitting states.

DOI: 10.1021/acs.jpcc.8b00841
J. Phys. Chem. C 2018, 122, 6463−6474

Table 1. Lifetime in ns (τ_1, τ_2, τ_3) and Pre-exponential Factor (in Parenthesis) of Each Decaying Component of the PL Decays Analyzed by Assuming a Triexponential Decay for CDs Embedded in a PMMA Solid Film, in Chloroform Solution, and in Toluene Solution[a,b]

	τ_1	τ_2	τ_3	τ_{av}
in PMMA film				
ex. 280 nm (obs. 330 nm)	0.324 (0.565)	1.88 (0.386)	11.7 (0.049)	1.48
ex. 280 nm (obs. 375 nm)	0.424 (0.528)	2.17 (0.345)	13.8 (0.127)	2.73
ex. 280 nm (obs. 450 nm)	0.431 (0.436)	2.32 (0.440)	9.71 (0.124)	2.41
ex. 380 nm (obs. 430 nm)	0.580 (0.401)	1.92 (0.514)	9.19 (0.085)	2.00
ex. 400 nm (obs. 457 nm)	0.600 (0.350)	1.88 (0.534)	8.45 (0.116)	2.19
in chloroform				
ex. 280 nm (obs. 330 nm)	0.072 (0.816)	0.623 (0.144)	2.42 (0.040)	0.25
ex. 280 nm (obs. 375 nm)	0.298 (0.577)	1.80 (0.335)	6.84 (0.088)	1.38
ex. 280 nm (obs. 450 nm)	0.386 (0.498)	2.07 (0.375)	7.79 (0.127)	1.96
ex. 380 nm (obs. 430 nm)	0.292 (0.579)	1.48 (0.357)	5.95 (0.064)	1.08
ex. 400 nm (obs. 457 nm)	0.281 (0.464)	1.52 (0.423)	5.56 (0.113)	1.40
in toluene				
ex. 280 nm (obs. 330 nm)	0.431 (0.699)	1.60 (0.235)	6.35 (0.066)	1.10
ex. 280 nm (obs. 375 nm)	0.376 (0.291)	2.18 (0.417)	8.05 (0.292)	3.37
ex. 280 nm (obs. 450 nm)	0.479 (0.360)	2.51 (0.434)	7.82 (0.206)	2.87
ex. 380 nm (obs. 430 nm)	0.332 (0.476)	1.69 (0.453)	6.73 (0.071)	1.40
ex. 400 nm (obs. 450 nm)	0.341 (0.408)	1.77 (0.475)	6.47 (0.117)	1.74

[a]The average lifetime (τ_{av}) is also given. [b]Experimental error is estimated to be ±15%.

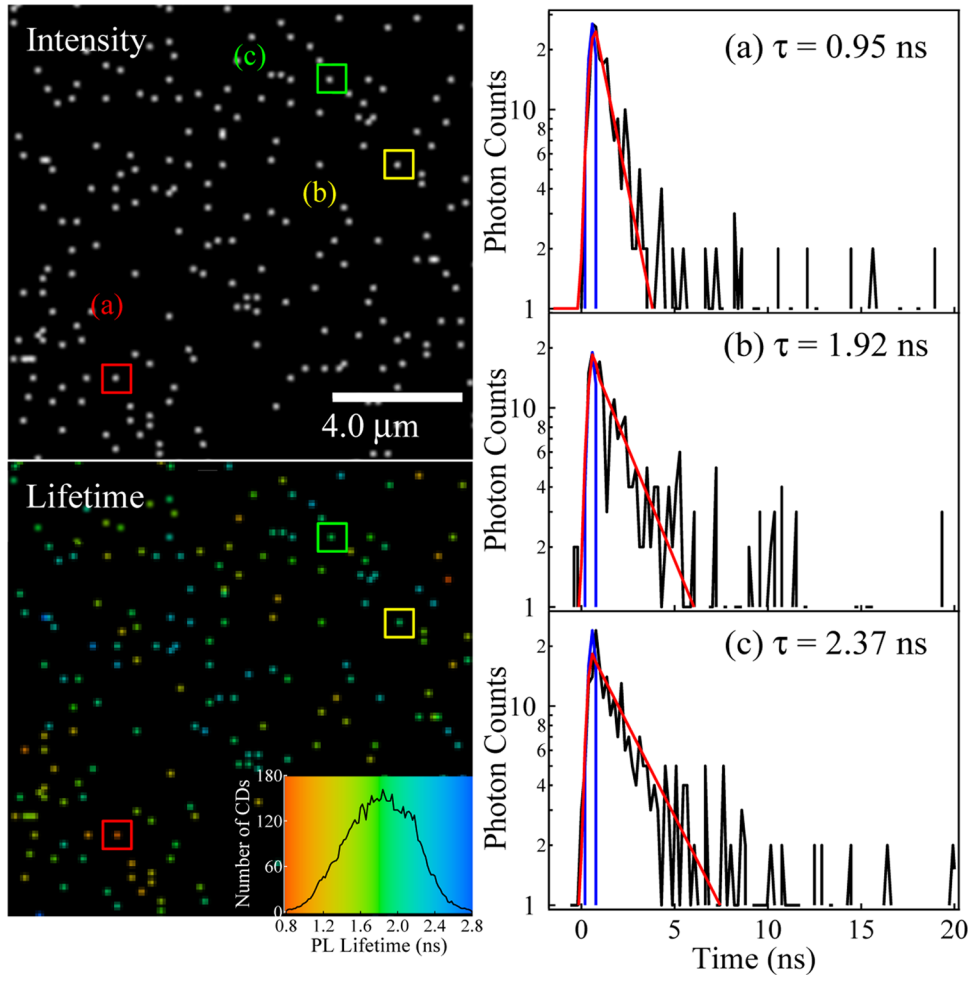

Figure 9. Fluorescence intensity image (left, top) and FLIM image (left, bottom), and fluorescence decay profiles observed at points (a)−(c) shown in the images. The histogram of the FLIM is also shown as inset in the FLIM image. Together with the decay profiles, scattered light profile (blue), simulated single exponential decay (red), and the evaluated lifetime are shown. Excitation was done at 385 nm, and PL in the region of 417−477 nm was monitored.

DOI: 10.1021/acs.jpcc.8b00841
J. Phys. Chem. C 2018, 122, 6463−6474

3.2. Electrophotoluminescence Measurements in a Solid Film.

Electric-field effects on the absorption spectra of CDs embedded in a PMMA solid film were examined, but clear E-A spectra of CDs could not be obtained, indicating that the field-induced change in absorption intensity relative to the absorption intensity, i.e., $\Delta A/A$, is less than 5×10^{-4} in the wavelength region of 260−400 nm. On the other hand, E-PL spectra of CDs in a PMMA film could be obtained with excitation at 280 nm with a field strength of 0.8 MV cm^{-1}. The results are shown in Figure 10. The field-induced change in PL intensity is proportional to the square of the applied electric field, as shown in Figure 11.

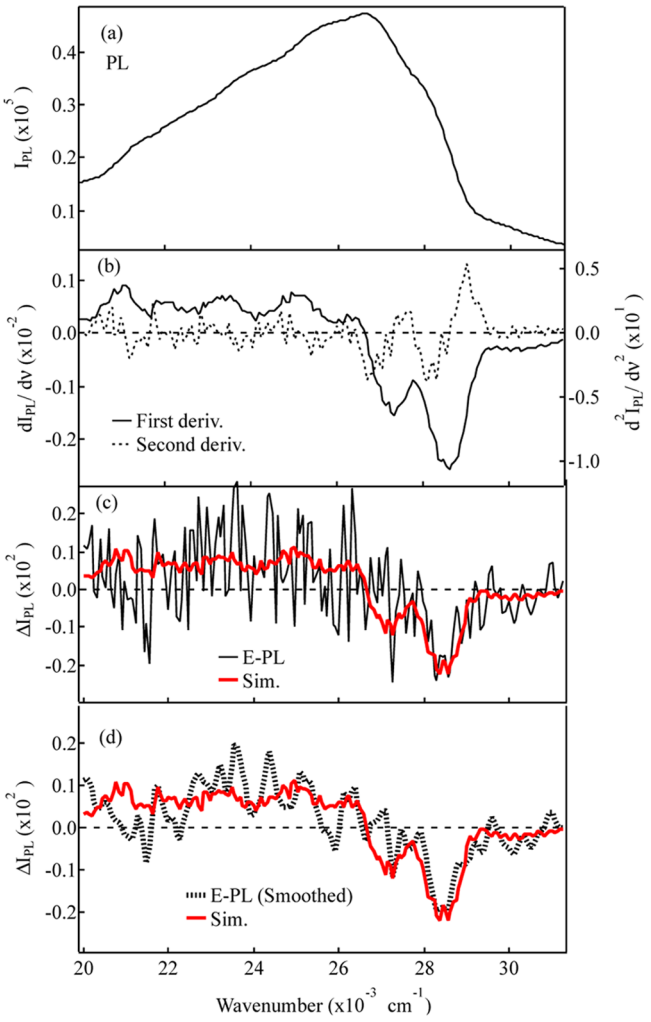

Figure 10. Spectra of CDs embedded in a PMMA solid film. (a) PL spectrum, (b) its first- and second-derivative spectra, (c) E-PL spectrum and simulated spectrum, and (d) E-PL spectrum smoothed over three points and simulated spectrum. The applied electric field was 0.8 MV cm^{-1}.

When an electric field (F) is applied to molecules or quantum dots, each energy level is shifted by $-\mu F - \alpha F^2/2$, where μ and α represent, respectively, the electric dipole moment and molecular polarizability of the state concerned. Due to this effect, the optical transition energy is shifted by $\Delta E = -\Delta\mu F - \Delta\alpha F^2/2$, where $\Delta\mu$ and $\Delta\alpha$ are the differences in μ and α, respectively, between the ground state (μ_g and α_g) and excited state (μ_e and α_e), i.e., $\Delta\mu = \mu_e - \mu_g$ and $\Delta\alpha = \alpha_e - \alpha_g$. According to the theory of electric field effects on optical

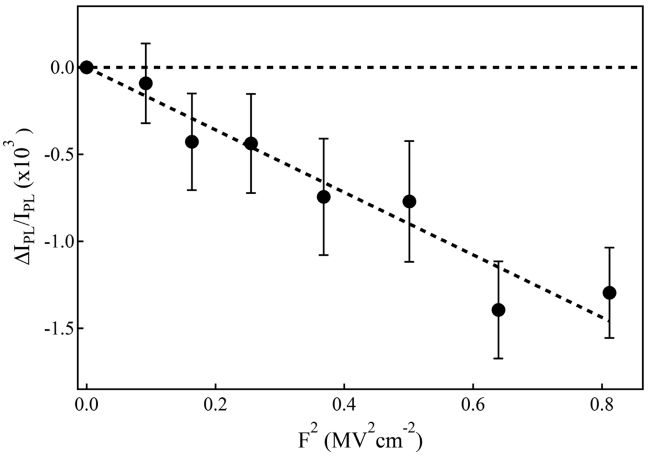

Figure 11. Plots of the field-induced change in PL intensity relative to the PL intensity as a function of the square of the applied electric field. The intensity was observed at 355 nm (28 200 cm^{-1}) with excitation at 280 nm. The dotted line is a guide to the eye.

spectra, the field-induced change in emission intensity at wavenumber ν, i.e., $\Delta I(\nu)$, is given by a linear combination of the zeroth, first, and second derivatives of the PL spectra given by $I_{PL}(\nu)$[34]

$$\Delta I_{PL}(\nu) = (fF)^2\left[A_\chi I_{PL}(\nu) + B_\chi \nu^3 \frac{d}{d\nu}\left\{\frac{I_{PL}(\nu)}{\nu^3}\right\} + C_\chi \nu^3 \frac{d^2}{d\nu^2}\left\{\frac{I_{PL}(\nu)}{\nu^3}\right\}\right] \quad (1)$$

where f and F represent the internal field factor and magnitude of applied electric field, respectively. In an immobilized and randomly distributed system, the zeroth-derivative coefficient A_χ originates from the field-induced change in emission intensity.

As in the case of electroabsorption spectra,[47−50] the first derivative coefficient B_χ and the second-derivative coefficient C_χ correspond to the spectral shift and spectral broadening of the E-PL spectra resulting from $\Delta\alpha$ and $\Delta\mu$, respectively. These coefficients are approximately expressed as follows

$$B_\chi \approx \frac{\Delta\bar{\alpha}}{2h}, \quad C_\chi \approx \frac{|\Delta\mu|^2}{6h^2} \quad (2)$$

where h represents Planck's constant and $\Delta\bar{\alpha}$ denotes the trace of $\Delta\alpha$, i.e., $\Delta\bar{\alpha} = (1/3)\,\mathrm{Tr}(\Delta\alpha)$. The values of $\Delta\bar{\alpha}$ and $|\Delta\mu|$ can be determined from eq 2, i.e., from the first- and second-derivative components of the E-PL spectrum, respectively.

As expected from eq 1, the E-PL spectra observed with a field of 0.8 MV cm^{-1} could be simulated by a linear combination of the zeroth, first, and second derivatives of the observed PL spectra, as shown in Figure 10. Emission intensity is very weak, and the signal-to-noise ratio of the E-PL spectrum is small. So, the E-PL spectrum averaged with three points is also shown in Figure 10d, together with the simulated spectrum. The coefficient of each derivative component determined from the simulated spectrum is shown in Table 2. On the basis of these coefficients, the values of $\Delta\mu$ and $\Delta\bar{\alpha}$ following emission are determined to be 2.2 ± 0.2 D and 38 ± 10 Å^3, respectively. These results suggest that CDs have a polar character in the excited state. The negligible intensity of the E-A spectra indicates that the radiative decay rate of CDs is little affected by

DOI: 10.1021/acs.jpcc.8b00841
J. Phys. Chem. C 2018, 122, 6463−6474

Table 2. Magnitude of the Change in Electric Dipole Moment ($\Delta\mu$) and Molecular Polarizability ($\Delta\bar{\alpha}$) Following Emission Process as Well as the Fitting Coefficients A_χ, B_χ, and C_χ in eq 1 for the E-PL Spectra Obtained with a Field Strength of 0.8 MV cm^{-1} [a]

	A_χ (MV^{-2} cm^2)	B_χ (MV^{-2} cm)	C_χ (MV^{-2})	$\Delta\bar{\alpha}$ (Å^3)	$\Delta\mu$ (D)
CD	1.25×10^{-4}	1.33	234	38	2.2

[a]Experimental error is estimated to be ±15%.

the application of F. Therefore, the fact that the zeroth-derivative component is slightly positive in the E-PL spectra indicates that PL intensity is slightly enhanced by the application of F, i.e., the nonradiative decay rate at the emitting state is de-enhanced by F.

In quite a large number of the so-called nonpolar molecules, nonzero values of electric dipole moment in the excited state have been reported[50−55] on the basis of the E-A measurements. In most of them, the charge localization following excitation into the charge-transfer state is considered as the main origin of the nonzero value of μ in the exited state. The charge localization may also occur in the local matrix field. The E-A spectra of C_{60} also show the nonzero value of the electric dipole moment in the excited state of C_{60} embedded in PMMA,[54] and the symmetry breaking was ascribed to a specific matrix effect, that is, nonsymmetrical interaction between C_{60} and the surrounding PMMA, in addition to the Jahn−Teller effect. The present E-PL spectra of CDs show that the value of $\Delta\mu$ is nonzero following emission. Although it is not certain whether the electric dipole moment is nonzero in either the ground or emitting state or in both states at the moment, the symmetry-breaking behavior of the E-PL spectra may result from the inhomogeneous interaction between CDs and the surrounding matrix of PMMA. The E-PL spectra of CDs were tried to be measured with excitation at 400 nm, but could not be observed because the emission intensity with excitation at 400 nm was not enough to obtain the E-PL spectra of PL(II).

4. CONCLUSIONS

Carbon nanodots (CDs) show two kinds of photoluminescence (PL) in both a PMMA solid film and solution: one is the emission with a peak at ∼375 nm (PL(I)), and another is the excitation-dependent emission, which shows the red shift of the peak, as the excitation wavelength becomes longer (PL(II)). PL excitation spectra observed by monitoring the emission at different wavelengths show that the bands located in the shorter wavelength below 280 nm are nearly independent of the monitoring wavelength, but the broad band located at wavelengths longer that 300 nm shifts to the red region with increasing the wavelength of the monitoring emission. The latter excitation peak corresponds to the absorption peak of PL(II), indicating that the emitting state of PL(II) is the real state at which direct absorption occurs from the ground state, not the transient trapped state produced by photoexcitation. Both PL(I) and PL(II) show a multiexponential decay in both solid film and solution. The average lifetime of PL(I), which is in the range of 1.3−3.5 ns, significantly depends on the environment; the average lifetime of PL(I) is much shorter in chloroform than in others, implying that the emitting state of PL(I) is related to the state where −COOH and −OH groups are ionized. The matrix effect on the average lifetime is significant in both PL(I) and PL(II); not only PL(I) but also PL(II) shows shorter average lifetime in chloroform than in toluene or in a PMMA film with excitation at 280 nm. The spectral shift during the passage of time following photoexcitation is not so large in any matrix, but the time-resolved PL spectra change in shape with the passage of time following photoexcitation at 280 nm because PL(I) and PL(II) show different lifetimes from each other. It is likely that the broadening of the PL(II) spectra results from the inhomogeneous PL characteristics of different CDs, but not due to the spectral migration following photoexcitation. Another PL component, which shows very short lifetime, is confirmed at 330 nm with excitation at 280 nm, which may be assigned to the hot luminescence emitted from higher vibrational levels of the emitting state. PL excitation spectra show strong intensity at wavelengths shorter than 300 nm in any matrix, suggesting that the intramolecular internal conversion from the photoexcited state to the lowest emitting state is very efficient in CDs, in agreement with the so-called Kasha's rule. FLIM images of CDs have been observed with excitation at 385 nm, and it is confirmed that multiple emitting states originate from the heterogeneous property of CDs. E-PL spectra could be also observed for PL(I) in a PMMA film, and the magnitude of the difference in electric dipole moment and in polarizability between the emitting state and the ground state has been determined. These results suggest that the emitting state of PL(I) has a dipolar character. In contrast to PL(I), the E-PL spectra of PL(II) could not be obtained probably because the signal is extremely small, suggesting that the difference in electric dipole moment and/or molecular polarizability between the emitting state of PL(II) and the ground state is very small.

■ ASSOCIATED CONTENT

Supporting Information

The Supporting Information is available free of charge on the ACS Publications website at DOI: 10.1021/acs.jpcc.8b00841.

X-ray diffraction (XRD) pattern of carbon nanodots and time-resolved PL spectra and intensity images in toluene with excitation at 280 nm and in chloroform with excitation at 400 nm (PDF)

■ AUTHOR INFORMATION

Corresponding Author

*E-mail: nohta@nctu.edu.tw.

ORCID

Toshifumi Iimori: 0000-0003-2158-4378
Eric Wei-Guang Diau: 0000-0001-6113-5679
Nobuhiro Ohta: 0000-0003-4255-6448

Notes

The authors declare no competing financial interest.

■ ACKNOWLEDGMENTS

This work was supported by Research Institute for Electronic Science, Hokkaido University, as a cooperative work under Chemical Network, Japan. This work was also supported by National Chiao Tung University and Ministry of Science and Technology (MOST, 106-2133-M-009-002) in Taiwan. The authors thank T. Tanaka for the measurements of the TEM images in the facility of Institute for Materials Chemistry and Engineering, Kyushu University, Japan.

DOI: 10.1021/acs.jpcc.8b00841
J. Phys. Chem. C 2018, 122, 6463−6474

REFERENCES

(1) Baker, S. N.; Baker, G. A. Luminescent Carbon Nanodots: Emergent Nanolights. *Angew. Chem., Int. Ed.* **2010**, *49*, 6726−6744.
(2) Shen, J.; Zhu, Y.; Yang, X.; Li, C. Graphene Quantum Dots: Emergent Nanolights for Bioimaging, Sensors, Catalysis and Photovoltaic Devices. *Chem. Commun.* **2012**, *48*, 3686−3699.
(3) Li, H.; Kang, Z.; Liu, Y.; Lee, S.-T. Carbon Nanodots: Synthesis, Properties and Applications. *J. Mater. Chem.* **2012**, *22*, 24230−24253.
(4) Chandra, S.; Das, P.; Bag, S.; Laha, D.; Pramanik, P. Synthesis, Functionalaization and Bioimaging Applications of Highly Fluorescent Carbon Nanoparticles. *Nanoscale* **2011**, *3*, 1533−1540.
(5) Yang, S.-T.; Cao, L.; Luo, P. G.; Lu, F.; Wang, X.; Wang, H.; Meziani, M. J.; Liu, Y.; Qi, G.; Sun, Y.-P. Carbon Dots for Optical Imaging in Vivo. *J. Am. Chem. Soc.* **2009**, *131*, 11308−11309.
(6) Cao, L.; Wang, X.; Meziani, M. J.; Lu, F.; Wang, H.; Luo, P. G.; Lin, Y.; Harruff, B. A.; Veca, L. M.; Murray, D.; et al. Carbon Dots for Multiphoton Bioimaging. *J. Am. Chem. Soc.* **2007**, *129*, 11318−11319.
(7) Wang, Q.; Zhang, C.; Shen, G.; Liu, H.; Fu, H.; Cui, D. Fluorescent Carbon Dots as an Efficient siRNA Nanocarrier for Its Interference Therapy in Gastric Cancer Cells. *J. Nanobiotechnol.* **2014**, *12*, 58.
(8) Bhunia, S. K.; Saha, A.; Maity, A. R.; Ray, S. C.; Jana, N. R. Cabon Nanoparticle-Based Fluorescent Bioimaging Probes. *Sci. Rep.* **2013**, *3*, No. 1473.
(9) Zhu, S.; Meng, Q.; Wang, L.; Zhang, J.; Song, Y.; Jin, H.; Zhang, K.; Sun, H.; Wang, H.; Yang, B. Highly Photoluminescent Carbon Dots for Multicolor Patterning, Sensors, and Bioimaging. *Angew. Chem.* **2013**, *125*, 4045−4049.
(10) Yu, S.-J.; Kang, M.-W.; Chang, H.-C.; Chen, K.-M.; Yu, Y.-C. Bright Fluorescent Nanodiamonds: No Photobleaching and Low Cytotoxicity. *J. Am. Chem. Soc.* **2005**, *127*, 17604−17605.
(11) Mitra, S.; Chandra, S.; Kundu, T.; Banerjee, R.; Pramanik, P.; Goswami, A. Rapid Microwave Synthesis of Fluorescent Hydrophobic Carbon Dots. *RSC Adv.* **2012**, *2*, 12129.
(12) Yang, Z.; Li, Z.; Xu, M.; Ma, Y.; Zhang, J.; Su, Y.; Gao, F.; Wei, H.; Zhang, L. Controllable Synthesis of Fluorescent Carbon Dots and Their Detection Application as Nanoprobes. *Nano-Micro Lett.* **2013**, *5*, 247−259.
(13) Bao, L.; Zhang, Z.-L.; Tian, Z.-Q.; Zhang, L.; Liu, C.; Lin, Y.; Qi, B.; Pang, D.-W. Electrochemical Tuning of Luminescent Carbon Nanodots: From Preparation to Luminescence Mechanism. *Adv. Mater.* **2011**, *23*, 5801−5806.
(14) Sun, Y.-P.; Zhou, B.; Lin, Y.; Wang, W.; Fernando, K. A. S.; Pathak, P.; Meziani, M. J.; Harruff, B. A.; Wang, X.; Wang, H.; et al. Quantum-Sized Carbon Dots for Bright and Colorful Photoluminescence. *J. Am. Chem. Soc.* **2006**, *128*, 7756−7757.
(15) Zhu, X.; Wang, H.; Jiao, Q.; Xiao, X.; Zuo, X.; Liang, Y.; Nan, J.; Wang, J.; Wang, L. Preparation and Characterization of the Fluorescent Carbon Dots Derived from the Lithium-Intercalated Graphite Used for Cell Imaging. *Part. Part. Syst. Charact.* **2014**, *31*, 771−777.
(16) Zuo, J.; Jiang, T.; Zhao, X.; Xiong, X.; Xiao, S.; Zhu, Z. Preparation and Application of Fluorescent Carbon Dots. *J. Nanomater.* **2015**, No. 787862.
(17) Zhou, J.; Sheng, Z.; Han, H.; Zou, M.; Li, C. Facile Synthesis of Fluorescent Carbon Dots Using Watermelon Peel as a Carbon Source. *Mater. Lett.* **2012**, *66*, 222−224.
(18) Hu, C.; Liu, Y.; Yang, Y.; Cui, J.; Huang, Z.; Wang, Y.; Yang, L.; Wang, H.; Xiao, Y.; Rong, J. One-Step Preparation of Nitrogen-Doped Graphene Quantum Dots from Oxidized Debris of Graphene Oxide. *J. Mater. Chem. B* **2013**, *1*, 39−42.
(19) Liang, Q.; Ma, W.; Shi, Y.; Li, Z.; Yang, X. Easy Synthesis of Highly Fluorescent Carbon Quantum Dots from Gelatin and Their Luminescent Properties and Applications. *Carbon* **2013**, *60*, 421−428.
(20) Zhou, L.; He, B.; Huang, J. Amphibious Fluorescent Carbon Dots: One-Step Green Synthesis and Application for Light-Emitting Polymer Nanocomposites. *Chem. Commun.* **2013**, *49*, 8078−8080.
(21) Wang, Q.; Zheng, H.; Long, Y.; Zhang, L.; Gao, M.; Bai, W. Microwave−Hydrothermal Synthesis of Fluorescent Carbon Dots from Graphite Oxide. *Carbon* **2011**, *49*, 3134−3140.
(22) Ray, S. C.; Saha, A.; Jana, N. R.; Sarkar, R. Fluorescent Carbon Nanoparticles: Synthesis, Characterization, and Bioimaging Application. *J. Phys. Chem. C* **2009**, *113*, 18546−18551.
(23) Zhu, H.; Wang, X.; Li, Y.; Wang, Z.; Yang, F.; Yang, X. Microwave Synthesis of Fluorescent Carbon Nanoparticles with Electroluminescence Properties. *Chem. Commun.* **2009**, 5118−5120.
(24) Zhou, J.; Booker, C.; Li, R.; Zhou, X.; Sham, T.-K.; Sun, X.; Ding, Z. An Electrochemical Avenue to Blue Luminescent Nanocrystals from Multiwalled Carbon Nanotubes (MWCNTs). *J. Am. Chem. Soc.* **2007**, *129*, 744−745.
(25) Liu, R.; Wu, D.; Liu, S.; Koynov, K.; Knoll, W.; Li, Q. An Aqueous Route to Multicolor Photoluminescent Carbon Dots Using Silica Spheres as Carriers. *Angew. Chem., Int. Ed.* **2009**, *48*, 4598−4601.
(26) Xu, X.; Ray, R.; Gu, Y.; Ploehn, H. J.; Gearheart, L.; Raker, K.; Scrivens, W. A. Electrophoretic Analysis and Purification of Fluorescent Single-Walled Carbon Nanotube Fragments. *J. Am. Chem. Soc.* **2004**, *126*, 12736−12737.
(27) Li, X.; Wang, H.; Shimizu, Y.; Pyatenko, A.; Kawaguchi, K.; Koshizuka, N. Preparation of Carbon Quantum Dots with Tunable Photoluminescence by Rapid Laser Passivation in Ordinary Organic Solvents. *Chem. Commun.* **2011**, *47*, 932−934.
(28) Ghosh, S.; Chizhik, A. M.; Karedla, N.; Dekaliuk, M. O.; Gregor, I.; Schuhmann, H.; Seibt, M.; Bodensiek, K.; Schaap, I. A. T.; Schulz, O.; et al. Photoluminescence of Carbon Nanodots: Dipole Emission Centers and Electron−Phonon Coupling. *Nano Lett.* **2014**, *14*, 5656−5661.
(29) Khan, S.; Gupta, A.; Verma, N. C.; Nandi, C. K. Time-Resolved Emission Reveals Ensemble of Emissive States as the Origin of Multicolor Fluorescence in Carbon Dots. *Nano Lett.* **2015**, *15*, 8300−8305.
(30) Sharma, A.; Gadly, T.; Gupta, A.; Ballal, A.; Ghosh, S. K.; Kumbhakar, M. Origin of Excitation Dependent Fluorescence in Carbon Nanodots. *J. Phys. Chem. Lett.* **2016**, *7*, 3695−3702.
(31) Callis, P. R.; Burgess, B. K. Tryptophan Fluorescence Shifts in Proteins from Hybrid Simulations: An Electrostatic Approach. *J. Phys. Chem. B* **1997**, *101*, 9429−9432.
(32) Park, E. S.; Andrews, S. S.; Hu, R. B.; Boxer, S. G. Vibrational Stark Spectroscopy in Proteins: A Probe and Calibration for Electrostatic Fields. *J. Phys. Chem. B* **1999**, *103*, 9813−9817.
(33) Kriegl, J. M.; Nienhaus, K.; Deng, P.; Fuchs, J.; Nienhaus, G. U. Ligand Dynamics in a Protein Internal Cavity. *Proc. Natl. Acad. Sci. U.S.A.* **2003**, *100*, 7069−7074.
(34) Ohta, N. Electric Field Effects on Photochemical Dynamics in Solid Films. *Bull. Chem. Soc. Jpn.* **2002**, *75*, 1637−1655.
(35) Umeuchi, S.; Nishimura, Y.; Yamazaki, I.; Murakami, H.; Yamashita, M.; Ohta, N. Electric Field Effects on Absorption and Fluorescence Spectra of Pyrene Doped in a PMMA Film. *Thin Solid Films* **1997**, *311*, 239−245.
(36) Tsushima, M.; Ushizaka, T.; Ohta, N. Time-Resolved Measurement System of Electrofluorescence Spectra. *Rev. Sci. Instrum.* **2004**, *75*, 479−485.
(37) Awasthi, K.; Nakabayashi, T.; Ohta, N. Effects of Nanosecond Pulsed Electric Field on Intracellular Function of HeLa Cells as Revealed by NADH Autofluorescence Microscopy. *ACS Omega* **2016**, *1*, 396−406.
(38) Awasthi, K.; Nakabayashi, T.; Li, L.; Ohta, N. Effects of Nanosecond Pulsed Electric Field on Intracellular NADH Autofluorescence: A Comparison between Normal and Cancer Cells. *ACS Omega* **2017**, *2*, 2916−2924.
(39) Wu, D.; Huang, X.; Deng, X.; Wang, K.; Liu, Q. Preparation of Photoluminescent Carbon Nanodots by Traditional Chinese Medicine and Application as a Probe for Hg^{2+}. *Anal. Methods* **2013**, *5*, 3023−3027.
(40) Li, F.; Liu, C.; Yang, J.; Wang, Z.; Liu, W.; Tian, F. Mg/N Double Doping Strategy to Fabricate Extremely High Luminescent Carbon Dots for Bioimaging. *RSC Adv.* **2014**, *4*, 3201−3205.

DOI: 10.1021/acs.jpcc.8b00841
J. Phys. Chem. C 2018, 122, 6463−6474

(41) Nguyen, V.; Si, J.; Yan, L.; Hou, X. Direct Demonstration of Photoluminescence Originated from Surface Functional Groups in Carbon Nanodots. *Carbon* **2016**, *108*, 268−273.
(42) Sui, L.; Jin, W.; Li, S.; Liu, D.; Jiang, Y.; Chen, A.; Liu, H.; Shi, Y.; Ding, D.; Jin, M. Ultrafast Carrier Dynamics of Carbon Nanodots in Different pH Environments. *Phys. Chem. Chem. Phys.* **2016**, *18*, 3838−3845.
(43) Liu, Y.; Liu, Y.; Park, M.; Park, S.-J.; Zhang, Y.; Akanda, M. R.; Park, B.-Y.; Kim, H. Y. Green Synthesis of Fluorescent Carbon Dots from Carrot Juice for in Vitro Cellular Imaging. *Carbon Lett.* **2017**, *21*, 61−67.
(44) Long, Y.-M.; Zhou, C.-H.; Zhang, Z.-L.; Tian, Z.-Q.; Bao, L.; Lin, Y.; Pang, D.-W. Shifting and Non-Shifting Fluorescence Emitted by Carbon Nanodots. *J. Mater. Chem.* **2012**, *22*, 5917−5920.
(45) Park, Y.; Yoo, J.; Lim, B.; Kwon, W.; Rhee, S.-W. Improving the Functionality of Carbon Nanodots: Doping and Surface Functionalization. *J. Mater. Chem. A* **2016**, *4*, 11582−11603.
(46) Yang, Y.; Cui, J.; Zheng, M.; Hu, C.; Tan, S.; Xiao, Y.; Yang, Q.; Liu, Y. One-Step Synthesis of Amino-Functionalized Fluorescent Carbon Nanoparticles by Hydrothermal Carbonization of Chitosan. *Chem. Commun.* **2012**, *48*, 380−382.
(47) Liptay, W. Dipole Moments and Polariabilities of Molecules in Excited Electronic States. In *Excited States*; Lim, E. C., Ed.; Academic Press: New York, 1974; Vol. *1*, pp 129−229.
(48) Jalviste, E.; Ohta, N. Theoretical Foundation of Electroabsorption Spectroscopy: Self-Contained Derivation of the Basic Equations with the Direction Cosine Method and the Euler Angle Method. *J. Photochem. Photobiol., C* **2007**, *8*, 30−46.
(49) Bublitz, G. U.; Boxer, S. G. Stark Spectroscopy: Applications in Chemistry, Biology, and Materials Science. *Annu. Rev. Phys. Chem.* **1997**, *48*, 213−242.
(50) Locknar, S. A.; Peteanu, L. A. Investigation of the Relationship between Dipolar Properties and Cis−Trans Configuration in Retinal Polyenes: A Comparative Study Using Stark Spectroscopy and Semiempirical Calculations. *J. Phys. Chem. B* **1998**, *102*, 4240−4246.
(51) Krawczyk, S.; Jaazurek, B.; Luchowski, R.; Wiacek, D. Electroabsorption Spectra of Caroteneoid Isomers: Conformational Modulation of Polarizability vs Induced Dipole Moments. *Chem. Phys.* **2006**, *326*, 465−470.
(52) Karki, L.; Hupp, J. T. Electroabsorption Studies of Metal-to-Ligand Charge Transfer in Ru(phenanthroline)$_3^{2+}$: Evidence for Intrinsic Charge Localization in the Initially Formed Excited State. *Inorg. Chem.* **1997**, *36*, 3318−3321.
(53) Ohta, N.; Iwaki, Y.; Ito, T.; Yamazaki, I.; Osuka, A. Photoinduced Charge Transfer along a Meso, Meso-Linked Porphyrin Array. *J. Phys. Chem. B* **1999**, *103*, 11242−11245.
(54) Ohta, N.; Tanaka, T.; Yamazaki, I. A Reduction of the High Symmetry of C_{60} in a PMMA Polymer Film as Revealed by Electroabsorption Spectra. *Res. Chem. Intermed.* **2001**, *27*, 61−71.
(55) Iimori, T.; Ito, R.; Ohta, N.; Nakano, H. Stark Spectroscopy of Rubrene. I. Electroabsorption Spectroscopy and Molecular Parameters. *J. Phys. Chem. A* **2016**, *120*, 4307−4313.

DOI: 10.1021/acs.jpcc.8b00841
J. Phys. Chem. C 2018, 122, 6463−6474